Motor transport of self-assembled cargos in crowded environments

Leslie Conway[a], Derek Wood[b], Erkan Tüzel[c], and Jennifer L. Ross[b,1]

[a]Molecular and Cellular Biology Graduate Program and [b]Department of Physics, University of Massachusetts, Amherst, MA 01003; and [c]Department of Physics, Worcester Polytechnic Institute, Worcester, MA 01609

Edited by Thomas D. Pollard, Yale University, New Haven, CT, and approved November 2, 2012 (received for review June 1, 2012)

Intracellular transport of cargo particles is performed by multiple motors working in concert. However, the mechanism of motor association to cargos is unknown. It is also unknown how long individual motors stay attached, how many are active, and how multimotor cargos would navigate a densely crowded filament with many other motors. Prior theoretical and experimental biophysical model systems of intracellular cargo have assumed fixed teams of motors transporting along bare microtubules or microtubules with fixed obstacles. Here, we investigate a regime of cargos transporting along microtubules crowded with free motors. Furthermore, we use cargos that are able to associate or dissociate motors as it translocates. We perform in vitro motility reconstitution experiments with high-resolution particle tracking. Our model system consists of a quantum dot cargo attached to kinesin motors, and additional free kinesin motors that act as traffic along the microtubule. Although high densities of kinesin motors hinder forward motion, resulting in a lower velocity, the ability to associate motors appears to enhance the run length and attachment time of the quantum dot, improving overall cargo transport. These results suggest that cargos that can associate new motors as they transport could overcome traffic jams.

axonal transport | cytoplasmic dynein

Intracellular transport is an essential cellular process used to move materials and information throughout the cell in an efficient manner (1, 2). Such transport is vital to the survival of long, extended animal cells, such as neurons, where diffusion is not adequate to deliver protein, organelles, and macromolecular cargos from the cell body to the active growing tips of cells (3, 4). Furthermore, the interior of the cell is highly crowded, yet active transport processes do not appear to jam or dissociate. Thus, motor-driven cargos must be able to circumvent traffic and crowding to efficiently deliver material throughout the cell.

Prior experimental and theoretical studies have resulted in many insights into the essential biological process of multiple motor cargo transport (5–11). For instance, it has been shown that association of multiple motors increases the run lengths of cargo, but does not affect the velocity under zero external load conditions (5–11). Additionally, experimental studies have shown that teams of motors are capable of bypassing static obstacles, such as microtubule-associated proteins or filament intersections, whereas single motors dissociate (6, 12–15).

Despite the vast gains in knowledge from these studies, there are still a number of open questions about intracellular transport. For instance, all of the above studies have focused on one or a few motors moving along bare microtubule tracks or tracks with static obstacles. Only recently has the idea of motor traffic been addressed experimentally and theoretically with single motors (16). Leduc et al. (16) examined a depolymerizing kinesin with long association times to assess the motile properties of single motors within high-density traffic jams along microtubules. However, no study has examined the effects of high-density traffic on cargos with multiple motors. Neither has any study examined cargos that could exchange or associate new motors.

In this study, we compared the motile properties of quantum dot (Qdot) cargos with that of single GFP-kinesin motors in densely crowded motor traffic on single microtubules. We found that both Qdot cargos and single GFP-kinesin motors display slower velocities with additional kinesin motor traffic. Using high-resolution tracking, we found that the Qdots slowed down due to pausing and a separate slower velocity. Because both Qdots and single-molecule kinesin motors slow their velocities to the same rates, we conclude that this activity is due to the higher traffic on the microtubule.

Interestingly, we found that Qdot cargos display longer run lengths and association times as the density of motors increases, whereas single kinesin motors displayed shorter run lengths. The main difference between a Qdot cargo and a single motor is the ability for the cargo to associate more than one motor; thus, the longer run lengths are due to multimotor association. Using two-color single-molecule imaging, we show that GFP-kinesin motors can associate to Qdots during motility to enhance the run length of the cargo.

Results

Crowding of Microtubules with Kinesin Motors. We visualized the density of kinesin motors by adding GFP-kinesin motors to the chamber at 5, 10, 25, 50, 100, and 200 nM (Fig. 1*A*). We quantified the linear motor density on the microtubules using the intensity of a single GFP-kinesin spot (clearly visible in Fig. 1*A*, 5 nM) and taking all images with the same exposure time and experimental conditions. We found that the binding of kinesin to the microtubule increases linearly with the kinesin concentration (Fig. 1*B*). Thus, we are in the low-binding regime where the free kinesin concentration is below the K_D value for kinesin binding in the presence of 0.5 mM ATP. We estimated the K_D value for kinesin binding to microtubules at 0.5 mM ATP from these images to be 60 nM (Fig. S1; see *SI Materials and Methods* for details).

Cargo and Single-Molecule Motility Are Affected by Crowding. We compared the motile properties of Qdot cargos to those of single GFP-kinesin motors while in the presence of increasing densities of kinesin motors from 1 to 200 nM. We created Qdot cargos by binding low concentrations of biotinylated kinesin motors to streptavidin-labeled Qdots. Qdot cargos or single GFP-kinesin motors were allowed to bind to microtubules in experimental flow chambers (complete methods are available in *SI Materials and Methods*). Excess, unlabeled kinesin was added to the system with 0.5 mM ATP. Qdots and single GFP-kinesins were visualized in total internal reflection fluorescence microscopy. Kymographs were used to identify moving particles, which were subsequently

Author contributions: L.C. and J.L.R. designed research; L.C. performed research; J.L.R. contributed new reagents/analytic tools; L.C., D.W., and J.L.R. analyzed data; and L.C., D.W., E.T., and J.L.R. wrote the paper.

The authors declare no conflict of interest.

This article is a PNAS Direct Submission.

[1]To whom correspondence should be addressed. E-mail: rossj@physics.umass.edu.

This article contains supporting information online at www.pnas.org/lookup/suppl/doi:10.1073/pnas.1209304109/-/DCSupplemental.

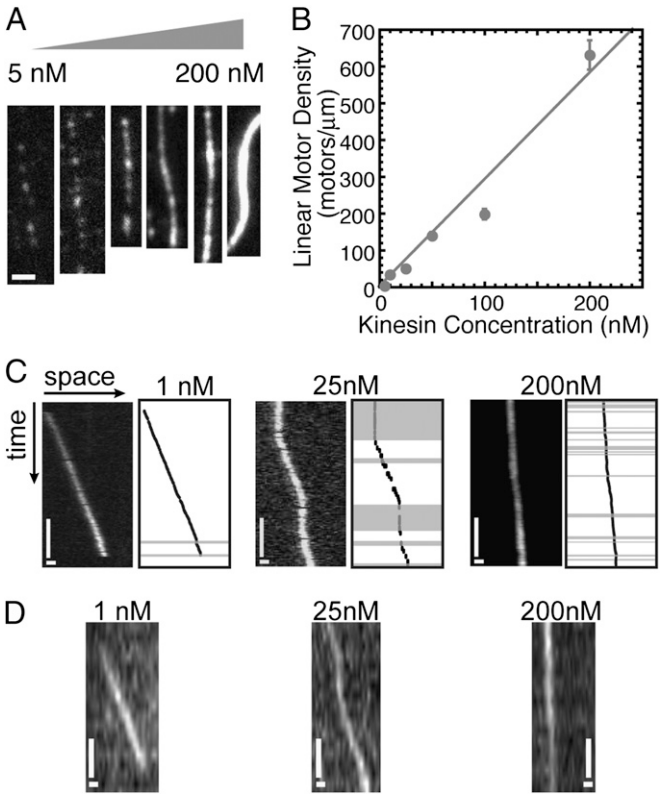

Fig. 1. Kinesin crowding and qualitative effects on Qdot and single GFP-kinesin motility. (*A*) Representative images of GFP-kinesin coating microtubules at 5, 10, 25, 50, 100, and 200 nM. Due to increasing levels of kinesin, these images are displayed with different linear look-up tables. For 5 and 10 nM, the gray scale is from 0 to 1,000 on 16-bit scale. For 25 nM, the gray scale is from 0 to 2,500. For 50 and 100 nM, the gray scale is from 0 to 5,000. For 200 nM, the gray scale is from 0 to 10,000, which is saturated. Single GFP-kinesin are clearly visible at 5 and 10 nM. (Scale bar, 1 μm.) (*B*) Linear motor density of GFP-kinesin along the microtubule as a function of added GFP-kinesin to the chamber. Error bars represent SEM for 50 microtubules analyzed for each density. The data fit to a line with one free slope parameter: $y = mx$. The best fit was achieved when $m = 2.9 \pm 0.2$, which gives a goodness of fit $R^2 = 0.96$. (*C*) Representative sections of kymographs for Qdot motility in the presence of 1, 25, and 200 nM added kinesin (not the entire kymograph run) on the left with the high-resolution trace on the right. Gray shading indicates periods of pausing determined using the threshold described. (Scale bars: vertical direction, 2 s; horizontal, 0.5 μm.) (*D*) Representative sections of kymographs for single GFP-kinesin in the presence of 1, 25, and 200 nM added kinesin. (Scale bars: vertical direction, 2 s; horizontal, 0.5 μm.)

tracked at high resolution (6–20 nm) using a centroid particle-tracking program (17–20) (Fig. 1*C*, Fig. S2). We were not able to track the GFP-kinesins with high resolution due to the low number of photons (Fig. 1*D*, Fig. S2).

We found that Qdot and single-molecule motility were both affected by the density of excess motors bound to the microtubule. The velocity of Qdots and single GFP-kinesin motors both slowed down when translocating along crowded microtubules. Velocity was quantified by dividing the total run length by the total time the cargo remained associated to the microtubule. On uncrowded microtubules (1 nM kinesin), Qdots and single GFP-kinesin motors displayed the same average velocity of 0.26 μm/s at 0.5 mM ATP used in our assays (Fig. 2*A*). As the density of additional kinesin increased on the microtubules, the velocities of Qdots and single GFP-kinesins both decreased until leveling off to a velocity of 0.076 μm/s at high crowding levels (Fig. 2*A*).

Qdots traveling on crowded microtubules exhibited pausing events during their runs (Fig. 1*C*). Our automated tracking program automatically identified pauses using a threshold on the velocity: velocity lower than 2 standard deviations (SDs) below the mean instantaneous velocity was considered paused (see *SI Materials and Methods*). To ensure that the decrease in velocity calculated is not an artifact of Qdots pausing more in crowded conditions, we calculated the velocity using only the segments of motion, omitting pauses from our calculation. As expected, omission of paused segments increased the measured velocity for all concentrations, but the trend for the velocity of the moving segments exactly mirrors that of the average velocity (Fig. 2*A*).

Despite the similar velocities of the Qdots and single GFP-kinesins, we found that the association time and run length of Qdot cargos were higher in the presence of kinesin traffic. At 1 nM, both GFP-kinesin and Qdots had an average run length of 1.76 μm (Fig. 2*B*). These data imply that the Qdots are being transported by single kinesins at 1 nM. At higher densities of kinesin on the microtubules, the run length of Qdots became longer, up to 6.23 μm at 200 nM (Fig. 2*B*). Oppositely, the run length of single GFP-kinesin motors in the presence of 200 nM unlabeled kinesin decreased to almost zero.

We observed a similar trend when we measured the total time of association. Qdots moving on uncrowded microtubules (1 nM kinesin) remained bound to the microtubule for an average of 8.23 s (Fig. 2*C*), and the association time increased to almost 100 s at 200 nM kinesin (Fig. 2*C*). Conversely, the association time of single GFP-kinesin motors was virtually unaffected by the crowding of other motors. Thus, traffic did not appear to alter the off rate of single motors (Fig. 2*C*).

Qdots Can Associate New Motor Attachments. Given the profound differences in motile properties between Qdots and single GFP-kinesins when confronted with kinesin traffic, there must be multiple motors associating with the Qdots during transport. Most strikingly, the difference in run length at the highest kinesin concentration (200 nM) reveals that the individual kinesin motors are moving only 0.1 μm, but the Qdots are moving for over 6 μm, a 60-fold increase in run length (Fig. 2*B*). Although most of our studies begin with a small number of kinesin motors affixed to the Qdots via biotin–streptavidin linkers, we found that this strong, specific attachment was not necessary for Qdot transport. Both non-biotinylated kinesin motors (unlabeled) and GFP-kinesin motors were able to associate to the Qdots to cause the same motility properties reported above (Fig. 3). Using two-color single-molecule imaging, we visualized dark red Qdots and single GFP-kinesins (5 nM) in a background of 50 nM excess unlabeled kinesin (Fig. 3 *A*–*F*).

We observed a variety of interactions between GFP-kinesin and Qdots, including adding new GFP-kinesins to the Qdot from the microtubule pool (Fig. 3 *A* and *B*) and dissociating GFP-kinesins from the Qdot (Fig. 3*C*). Some Qdots bound to the microtubule with a GFP-kinesin already attached (Fig. 3*D*) and others were observed to dissociate with GFP-kinesin bound (Fig. 3*E*). Some Qdots associated to GFP-kinesins that were already moving along the microtubule, and they moved together (Fig. 3*F*). Interestingly, we often observe that, when a new kinesin associates with the Qdot, the Qdot begins to move from a pause (Fig. 3 *A* and *B*).

At 50 nM background kinesin, the run length of Qdots was over 4.5 μm, whereas the run length of single GFP-kinesins not attached to Qdots was only 1 μm (Fig. 2*B*). These single GFP-kinesins are easily visualized along with the Qdot bound kinesins (Fig. 3). GFP-kinesins on the Qdot have a longer association time and run length than single motors observed on the same microtubule, implying that they stay attached to the Qdot for longer

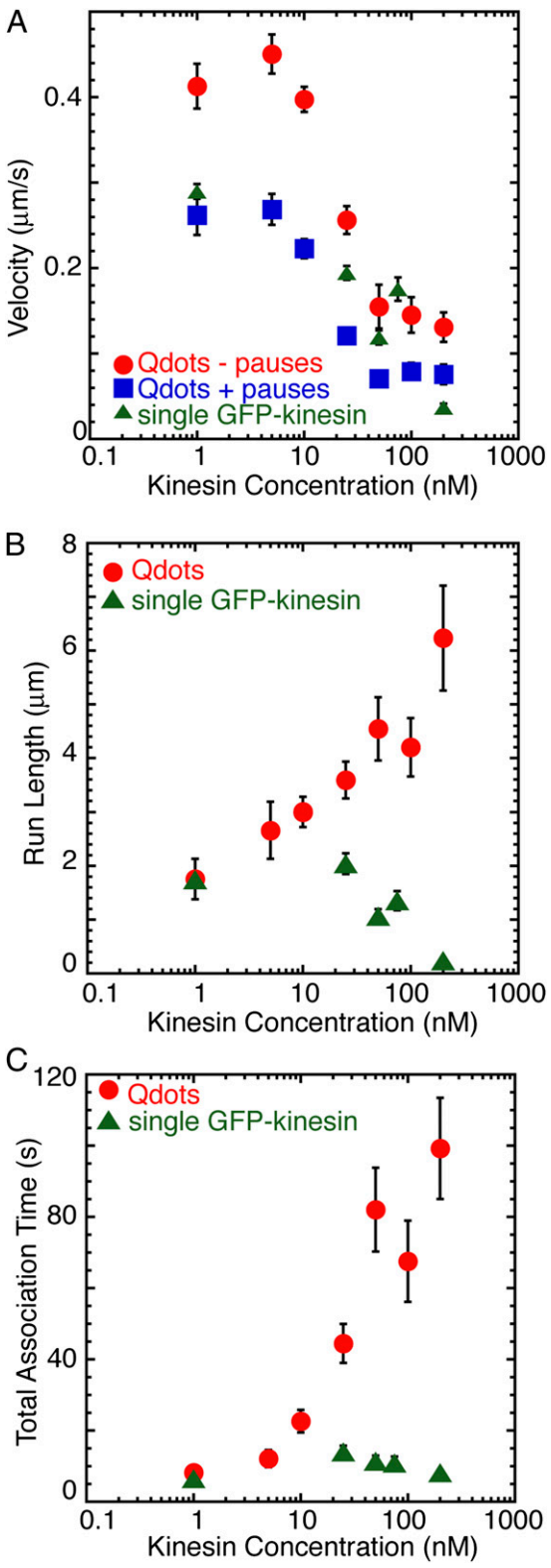

Fig. 2. Motility properties of Qdot cargos and single GFP-kinesin motors under increasingly crowded conditions. (*A*) Velocity was measured in two ways: the overall velocity of each individual cargo such that all pauses were included in the measurement (blue squares) and the velocity of each individual cargo where only the moving portions of the run were measured such that all pause events were omitted from this measurement (red circles). These data show that the drop in velocity observed, as conditions become more crowded, cannot be attributed only to an increase in pausing [1 nM (n = 19); 5 nM (n = 36); 10 nM (n = 138); 25 nM (n = 106); 50 nM (n = 49); 100 nM (n = 22); 200 nM (n = 36)]. Velocity for single GFP-kinesin is shown (green triangles) [1 nM (n = 101); 25 nM (n = 104); 50 nM (n = 55); 75 nM (n = 54); 200 nM (n = 103)]. (*B*) Run length was measured as the total distance traveled along the microtubule by a Qdot cargo (red circles) [1 nM (n = 19); 5 nM (n = 36); 10 nM (n = 138); 25 nM (n = 106); 50 nM (n = 49); 100 nM (n = 22); 200 nM (n = 36)]. Run length for single GFP-kinesin is shown (green triangles) [1 nM (n = 101), 25 nM (n = 104); 50 nM (n = 55); 75 nM (n = 54); 200 nM (n = 103)]. (*C*) Association time was measured as the total time that a single cargo spent bound to the microtubule (red circles) [1 nM (n = 19); 5 nM (n = 36); 10 nM (n = 138); 25 nM (n = 106); 50 nM (n = 49); 100 nM (n = 22); 200 nM (n = 36)]. Association time for single GFP-kinesin is shown (green triangles) [1 nM (n = 101); 25 nM (n = 104); 50 nM (n = 55); 75 nM (n = 54); 200 nM (n = 103)]. Error bars represent SEM for all plots.

than anticipated by quantification of the equilibrium dissociation constant (Fig. S3).

We measured the number of GFP-kinesins bound to each Qdot (Fig. 3*G*). The number of GFP-kinesins on each Qdot is best fit with a binomial distribution of the following form: $\binom{N}{n}p^n(1-p)^{N-n}$, where n is the number of GFP-kinesins on the Qdots measured, p is the probability of choosing a GFP-kinesin, and N is the number of sites where kinesin can bind. We know that p is 10% because we added 5 nM labeled GFP-kinesin to a total of 50 nM kinesin. Our unknown parameter is N. We find the best fit occurs when N equals 7 (R^2 is 0.89), implying that there are likely seven total kinesins bound on each Qdot under these conditions (50 nM). Because the Qdots are able to associate GFP-kinesins nonspecifically, they are effectively self-assembling as cargos.

Crowded Conditions Cause Pausing. Qdot cargos displayed a high number of pauses as they were transported along microtubules (Fig. 1*C*), which we automatically identified and quantified using our high-resolution tracking program. We found that Qdots spent more total time paused per run as a function of the concentration of added kinesin (Fig. 4*A*). We measured the temporal and spatial pause frequency (s^{-1} and μm^{-1}, respectively) as a function of added kinesins. We found that both the temporal (gray circles) and spatial (black circles) pause frequencies increased as microtubules became more crowded with similar trends (Fig. 4*B*).

We measured the individual pause durations for cargos transported on uncrowded microtubules (1 nM), microtubules with intermediate levels of crowding (25 nM kinesin), and microtubules with high levels of crowding (200 nM kinesin) as determined automatically from our tracking program. We found that the distribution of pause durations were exponential decays (Fig. 4*C*). We fit each distribution to an exponential decay function: $y = A\exp(-t/\tau)$. We found that the characteristic decay time, τ, decreased linearly with the log of kinesin-1 concentration (Fig. 4*D*). We replotted the distributions as cumulative probability distributions to show that these distributions are distinct. The cumulative distributions fit to the exponential cumulative probability distribution function well (Fig. S4). This implies that, although the number of pauses is increasing, the duration of each pause decreases.

Crowded Conditions Cause Qdot Reversals. In a number of the Qdot cargo tracks analyzed, we observed short, subpixel reversals. Fig. 5*A* depicts an example of a kymograph in which a reverse event occurs along with the high-resolution track overlaid. The arrow indicates the point in the run where the cargo reverses direction. Although these reversal events are difficult to distinguish in raw kymographs, the high-resolution tracking program was able to pick the reverse events that moved with negative velocity over a threshold distance of 50 nm without bias. The 50-nm threshold is eightfold greater than the resolution for events on this timescale

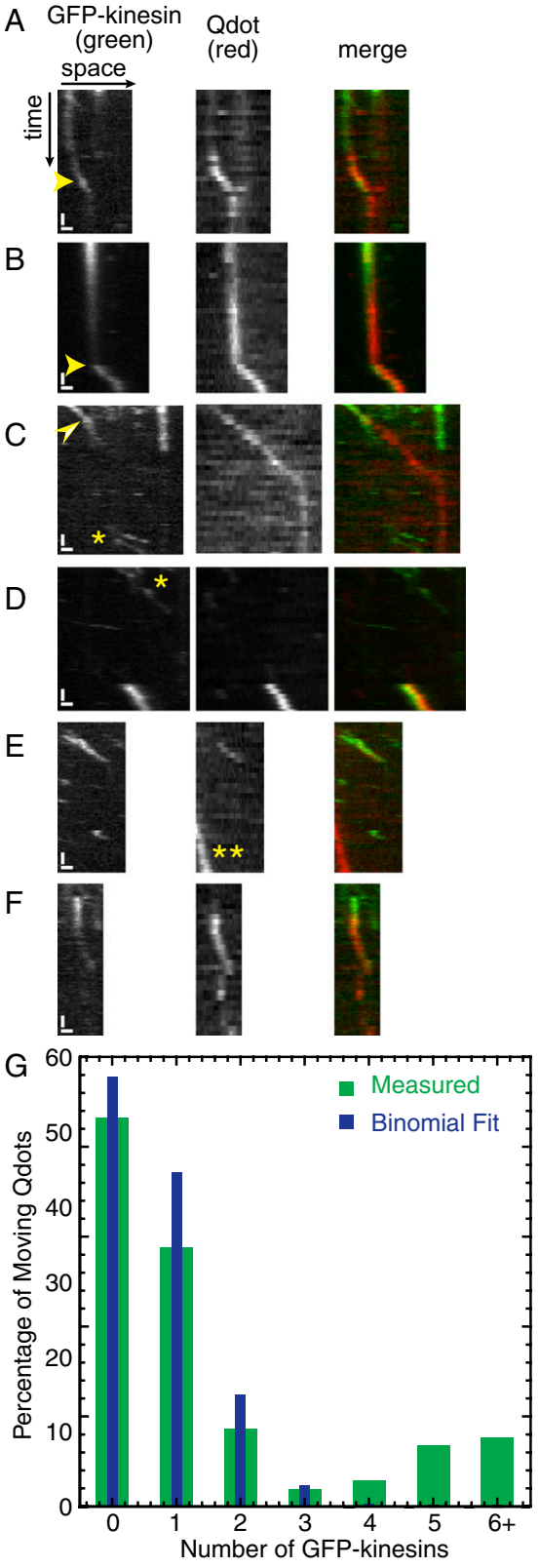

Fig. 3. Two-color single-molecule assays show association and dissociation of kinesin motors to Qdots. (*A–F*) Example kymographs depicting various ways in which Qdots were observed to associate or dissociate GFP-kinesin motors while translocating along the microtubule. Left kymographs show GFP-kinesin motility (green in merge), middle kymographs show Qdot motility (red in merge), and right kymographs show the merge of the two channels. (Scale bars: vertical direction, 10 s; horizontal direction, 0.5 μm.) (*A* and *B*) GFP-kinesin motor is observed to associate with a Qdot already bound to the microtubule. A yellow arrowhead indicates GFP-kinesin binding event. (*C*) GFP-kinesin motor is observed to dissociate from a Qdot while the Qdot is moving along the microtubule. A yellow arrowhead indicates GFP-kinesin dissociation event. (*D*) Qdot and GFP-kinesin are observed to bind the microtubule simultaneously. Single GFP-kinesin motors traveling on the same microtubule are also observed (*). (*E*) Qdot and GFP-kinesin are observed to dissociate from the microtubule simultaneously. Unlabeled kinesin motors transport a second Qdot (**). (*F*) Qdot is observed to bind directly to a GFP-kinesin already bound to the microtubule. (*G*) Histogram representing the number of GFP-kinesin motors bound to Qdots. The green bars represent data measured from the two-color assays. The blue bars represent the binomial fit used to estimate the number of kinesin binding spots available on the Qdot.

(<6 nm). To ensure that reversals counted were real and above the noise, stationary particles were analyzed with the particle-tracking program to determine the number of reversals due to system noise. From this control, we found that the program determined that 5% of stationary particles reversed over the duration of the movie. Moving Qdots were more likely than stationary Qdots to display reversals. Furthermore, the number of Qdots displaying at least one reversal event is a linear function of the log kinesin concentration added to crowd the microtubule (Fig. 5*B*, R^2 is 0.95).

We found no dependence of reverse frequency (temporal or spatial) on motor number (Fig. S5). We also found that there was no dependence of the reversal distance as a function of motor concentration by comparing histograms of reversal distance for 1, 25, and 200 nM kinesin (Fig. S5). All distributions were exponential decays with almost identical decay lengths. Thus, the characteristics of the reversals we observe do not depend on the motor number, only the likelihood that a cargo would reverse increased as the motor number increased.

Discussion

We have determined the motile properties for Qdots that can self-assemble into transport cargos by binding motor proteins nonspecifically. These artificial cargos allow us to test the hypotheses of several theoretical models of intracellular transport in the presence of crowding by other motors. We found that the run length and association time of the cargo are longer when the density of additional kinesin motors on the microtubule is higher, implying that the cargo has multiple motors bound. Single-molecule GFP-kinesins have decreasing run length and constant association time as the crowding increases. The differences between Qdots and single GFP-kinesins are especially pronounced at 200 nM of additional kinesin. Using two-color microscopy, we found that GFP-kinesins can nonspecifically bind to Qdots and stay bound to the microtubule longer when coupled into the cargo complex than when they are single motors. Furthermore, we observe that motors can associate and dissociate from the Qdot as it moves.

Multiple motors attached to the Qdot cause the altered behavior of Qdots compared with single GFP-kinesin motors. As shown in previous experimental (7, 21) and theoretical studies (8, 9, 11, 22), the more motors that are attached to a cargo, the farther the cargo can travel along the microtubule. Particularly, for relatively small cargo such as a Qdot, forces due to fluctuations dominate, and motor dissociation from the track is a Poissonian process. The lowered frictional load also reduces the escape rate of a motor, decreasing the likelihood of detachment before another motor attaches (9). Our observed run lengths of cargos transported in the presence of 50 nM kinesin are consistent with earlier theoretical predictions of 4–6 μm, for cargo carried by a maximum of one to three molecular motors (8, 9). We directly observe that there are likely seven motors bound to each Qdot using our two-color assay (Fig. 3). There are several explanations

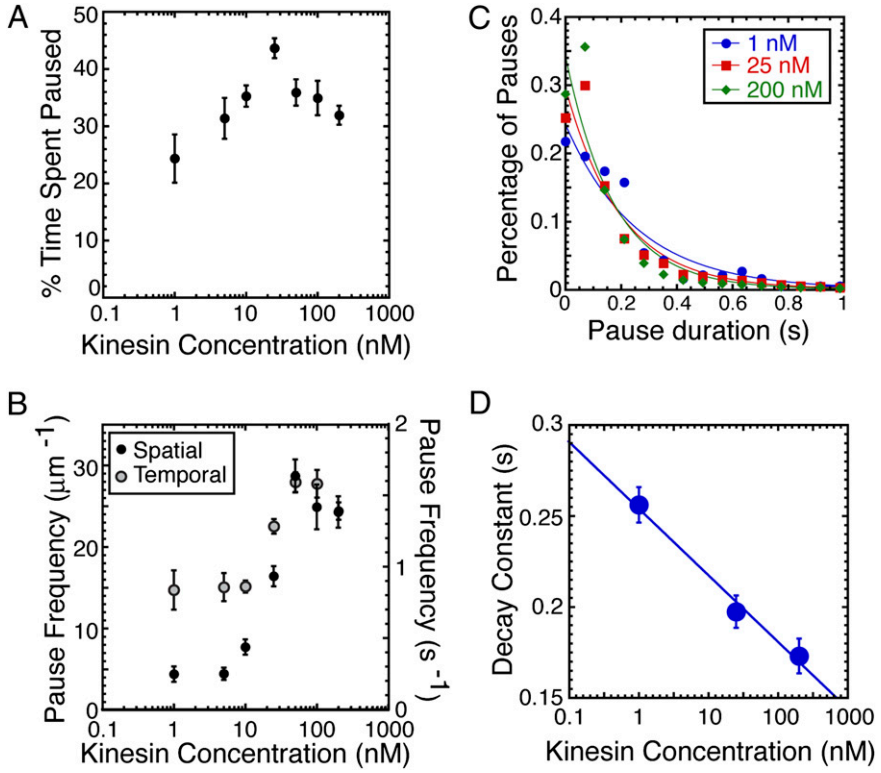

Fig. 4. Characteristics of pausing of Qdot cargos. (*A*) Percentage of time spent paused is measured as the percentage of time each individual cargo spent paused during its entire association time [1 nM ($n = 19$); 5 nM ($n = 36$); 10 nM ($n = 138$); 25 nM ($n = 106$); 50 nM ($n = 49$); 100 nM ($n = 22$); 200 nM ($n = 36$)]. Error bars represent SEM. (*B*) Spatial pause frequency (black circles) and temporal pause frequency (gray circles) are a measure of the average number of times a single cargo pauses per micrometer per run or per second per run, respectively [1 nM ($n = 19$); 5 nM ($n = 36$); 10 nM ($n = 138$); 25 nM ($n = 106$); 50 nM ($n = 49$); 100 nM ($n = 22$); 200 nM ($n = 36$)]. Error bars represent SEM. (*C*) Normalized distribution of the pause duration (in seconds) for cargos in the presence of 1 nM (blue circles, line), 25 nM (red squares, line), and 200 nM (green diamonds, line) with exponential decay fits represented by the same color line. Characteristic decay times for each distribution are as follows: 0.21 ± 0.03 s for 1 nM ($R^2 = 0.92$), 0.117 ± 0.007 for 25 nM ($R^2 = 0.99$), and 0.088 ± 0.004 for 200 nM ($R^2 = 0.995$). (*D*) The decay constant found from the exponential decay fits of *C* are plotted as a function of kinesin crowding concentration and found to decay linearly with the log of the concentration. We fit the function: $y = m$ (log (C)) + b to the function and found $m = -0.037 \pm 0.004$, $b = 0.25 \pm 0.006$ ($R^2 = 0.99$).

for this discrepancy. First, some of the bound motors may not be actively walking, but rather acting as additional cargo attached to the Qdot. Second, the prior work was performed with cargos with multiple motors but without additional high-density traffic that could act to reduce the run lengths below expected values.

We observe an interesting dependence of the run length, association time, and the reversal probability as a function of increasing density of kinesin. Specifically, each of these parameters is a linear function of the log of the added kinesin concentration. Logarithmic functions grow slower than linear functions and appear to saturate instead of steadily rising. Previous theoretical studies showed that the run length of cargos should increase linearly with the number of motors bound to the bead (8, 9). In our system, the additional motors are not only bound to the bead but are also acting as traffic to impede forward motion. Prior experimental and theoretical work show that, as the traffic density grows, the association time and run length decrease for single motors (16). In our system, we have both more motors on the Qdot that enhance run length, and higher density traffic motors that decrease run length. These two effects compete, but the impeding traffic is more effective because the small Qdots have limited space to add more motors. Thus, the run length and association time of the cargos only grow logarithmically, instead of linearly. The same effect is likely causing the logarithmic dependence of the probability of reversal.

The density of added motors is likely causing the pausing and reversal effects observed for Qdots, as well. Despite the growing number of pausing events, each pause becomes shorter with more motors (Fig. 4). These seemingly conflicting results are likely due to the antagonistic effects of having more motors per cargo and more traffic. Increasing the number of motors enables the cargo to interact with several protofilaments of the microtubule, which could enable the cargo to pass traffic on a paused protofilament. This is similar to changing lanes in a vehicular traffic jam. Despite this flexibility to change lanes, the likelihood of encountering a jammed path increases with motor density, causing more pauses.

Another unique observation in the motility of self-assembled cargos is short reversals. The reversals are very short, subpixel, but they do exist above the noise floor measured for stationary Qdots (Fig. 5*B*). Because the number of reversals is linearly proportional to the log of the density of kinesin motors crowding the filament, we conclude that reversals are being triggered by crowding on the filament. Unlike pausing, the frequency and distance of reversals do not depend on the crowding conditions. This implies that all reversals are identical. We conjecture that all of the reversals are the same and may be caused by "bead flop." Bead flop occurs when the front motor detaches and the center of the bead repositions backward. A previous experimental study of multimotor motility showed backward jumps that were likely the same mechanism as the bead flop we are detecting (21). Bead flop can only occur in multiple motor systems because single motors would cause the dissociation of the entire Qdot. We would expect more bead flop to occur as more Qdots have multiple motors.

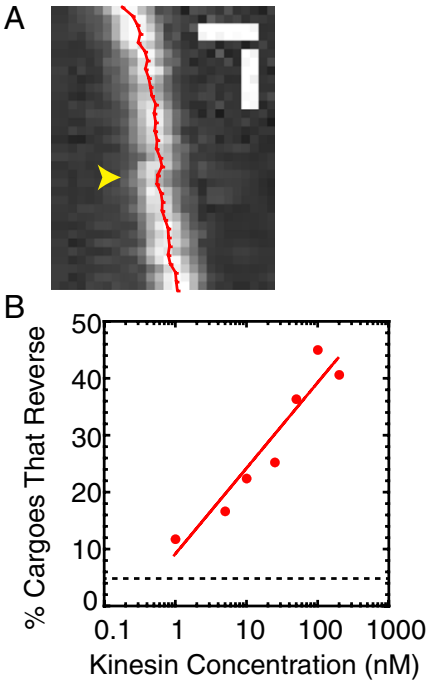

Fig. 5. Crowding and multiple motors on cargos results in short reversal motions. (*A*) The kymograph depicts the track of a single cargo carried by kinesin-1 in crowded conditions (50 nM kinesin-1). The arrow indicates the point during the run where the cargo reverses. The red line kymograph overlay was generated by the high-resolution tracking program used to analyze all data. Each point represents the localization of the cargo in each frame of the movie. The data were not smoothed. (Scale bars: vertical, 0.5 s; horizontal, 0.5 μm.) (*B*) The plot shows the percentage of cargos that reverse at least once per run. The 5% dashed line represents the noise floor of our measurement for stationary Qdots. We fit the data to a linear fit of the log of the density of kinesin: $y = m^*\log(x) + b$, where $m = 8 \pm 3$ and $b = 15 \pm 2$.

The work presented here explores a parameter space for intracellular traffic, specifically the activity of cargo in crowded conditions. Our artificial cargo can associate multiple motors, which aids in extending the association time and run length of the cargo at motor densities when single motors rapidly dissociate. These results are very important for the transport of intracellular cargos that need to transport long distances in crowded spaces, especially in elongated cells, such as neurons. Recent work on slow axonal transport has shown that proteinaceous material transiently assembles with kinesin motors to be transported quickly for short times (23). We do observe that, when a new kinesin motor binds to the Qdot, it is able to move faster (Fig. 3). This is reminiscent of the short-term fast transport observed for slow axonal transport particles (23, 24). Thus, the ability to associate and dissociate kinesin motors, as our Qdot cargos appear to, may be of biological significance to slow axonal transport. Future studies of other regimes are still needed to completely understand and recapitulate intracellular cargo transport. For instance, both myosin-V and kinesin-1 can fold up and autoinhibit (25–28). It is unknown how such regulation would affect unidirectional and bidirectional cargo transport. The system we created here may be a first step to begin to address these future interesting avenues.

Materials and Methods

Detailed materials and methods can be found in *SI Materials and Methods*.

To label Qdots with HaloTag kinesin, we used the HaloTag PEG-Biotin Linker (Promega) that covalently binds the HaloTag to generate a biotinylated kinesin. Qdot streptavidin conjugates, 525-nm emission (Invitrogen), were then bound to the kinesin. HaloTag kinesin, HaloTag PEG-Biotin Linker, and Qdot streptavidin conjugates were mixed in a 1:10:10 ratio, respectively, to ensure only one kinesin molecule per Qdot. HaloTag kinesin and HaloTag PEG-Biotin Linker were incubated together first for 10 min at room temperature. Qdot streptavidin conjugates were then added and incubated for an additional 10 min at room temperature. Complexes were then kept on ice.

ACKNOWLEDGMENTS. We thank C. Fagerstrom for tubulin purification and Kristopher E. Daly and Andrew M. O' Neill for useful discussions. L.C. was supported by the Institute for Cellular Engineering, National Science Foundation (NSF) Integrative Graduate Education and Research Traineeship Program Grant DGE-0654128, NSF Grant CMMI-0928540 (to J.L.R.), and a March of Dimes Basil O'Connor Award (to J.L.R.). J.L.R. and D.W. were supported by NSF Major Research Instrumentation Program Grant DBI-0923318. A Cottrell Scholars Award from Research Corporation for Science Advancement (to J.L.R.) also supported this work. E.T. was supported by the Eppley Foundation for Research and Worcester Polytechnic Institute start-up funds.

1. Ross JL, Ali MY, Warshaw DM (2008) Cargo transport: Molecular motors navigate a complex cytoskeleton. *Curr Opin Cell Biol* 20(1):41–47.
2. Caviston JP, Holzbaur EL (2006) Microtubule motors at the intersection of trafficking and transport. *Trends Cell Biol* 16(10):530–537.
3. Chevalier-Larsen E, Holzbaur EL (2006) Axonal transport and neurodegenerative disease. *Biochim Biophys Acta* 1762(11–12):1094–1108.
4. Hammond JW, Griffin K, Jih GT, Stuckey J, Verhey KJ (2008) Co-operative versus independent transport of different cargoes by Kinesin-1. *Traffic* 9(5):725–741.
5. Beeg J, et al. (2008) Transport of beads by several kinesin motors. *Biophys J* 94(2): 532–541.
6. Vershinin M, Xu J, Razafsky DS, King SJ, Gross SP (2008) Tuning microtubule-based transport through filamentous MAPs: The problem of dynein. *Traffic* 9(6):882–892.
7. Vershinin M, Carter BC, Razafsky DS, King SJ, Gross SP (2007) Multiple-motor based transport and its regulation by Tau. *Proc Natl Acad Sci USA* 104(1):87–92.
8. Kunwar A, Vershinin M, Xu J, Gross SP (2008) Stepping, strain gating, and an unexpected force-velocity curve for multiple-motor-based transport. *Curr Biol* 18(16): 1173–1183.
9. Korn CB, Klumpp S, Lipowsky R, Schwarz US (2009) Stochastic simulations of cargo transport by processive molecular motors. *J Chem Phys* 131(24):245107.
10. Mallik R, Petrov D, Lex SA, King SJ, Gross SP (2005) Building complexity: An in vitro study of cytoplasmic dynein with in vivo implications. *Curr Biol* 15(23):2075–2085.
11. Klumpp S, Nieuwenhuizen TM, Lipowsky R (2005) Self-organized density patterns of molecular motors in arrays of cytoskeletal filaments. *Biophys J* 88(5):3118–3132.
12. Dixit R, Ross JL, Goldman YE, Holzbaur EL (2008) Differential regulation of dynein and kinesin motor proteins by tau. *Science* 319(5866):1086–1089.
13. Ross JL, Shuman H, Holzbaur EL, Goldman YE (2008) Kinesin and dynein-dynactin at intersecting microtubules: Motor density affects dynein function. *Biophys J* 94(8): 3115–3125.
14. Seitz A, Surrey T (2006) Processive movement of single kinesins on crowded microtubules visualized using quantum dots. *EMBO J* 25(2):267–277.
15. Telley IA, Bieling P, Surrey T (2009) Obstacles on the microtubule reduce the processivity of Kinesin-1 in a minimal in vitro system and in cell extract. *Biophys J* 96(8):3341–3353.
16. Leduc C, et al. (2012) Molecular crowding creates traffic jams of kinesin motors on microtubules. *Proc Natl Acad Sci USA* 109(16):6100–6105.
17. Thompson RE, Larson DR, Webb WW (2002) Precise nanometer localization analysis for individual fluorescent probes. *Biophys J* 82(5):2775–2783.
18. Dahan M, et al. (2003) Diffusion dynamics of glycine receptors revealed by single-quantum dot tracking. *Science* 302(5644):442–445.
19. Ali MY, Lu H, Bookwalter CS, Warshaw DM, Trybus KM (2008) Myosin V and Kinesin act as tethers to enhance each others' processivity. *Proc Natl Acad Sci USA* 105(12):4691–4696.
20. Gao Y, Kilfoil ML (2009) Accurate detection and complete tracking of large populations of features in three dimensions. *Opt Express* 17(6):4685–4704.
21. Leduc C, Ruhnow F, Howard J, Diez S (2007) Detection of fractional steps in cargo movement by the collective operation of kinesin-1 motors. *Proc Natl Acad Sci USA* 104(26):10847–10852.
22. Müller MJ, Klumpp S, Lipowsky R (2010) Bidirectional transport by molecular motors: Enhanced processivity and response to external forces. *Biophys J* 98(11):2610–2618.
23. Scott DA, Das U, Tang Y, Roy S (2011) Mechanistic logic underlying the axonal transport of cytosolic proteins. *Neuron* 70(3):441–454.
24. Brown A (2003) Axonal transport of membranous and nonmembranous cargoes: A unified perspective. *J Cell Biol* 160(6):817–821.
25. Liu Y, Guo Y, Valles JM, Jr., Tang JX (2006) Microtubule bundling and nested buckling drive stripe formation in polymerizing tubulin solutions. *Proc Natl Acad Sci USA* 103(28):10654–10659.
26. Thirumurugan K, Sakamoto T, Hammer JA, 3rd, Sellers JR, Knight PJ (2006) The cargo-binding domain regulates structure and activity of myosin 5. *Nature* 442(7099):212–215.
27. Kaan HY, Hackney DD, Kozielski F (2011) The structure of the kinesin-1 motor-tail complex reveals the mechanism of autoinhibition. *Science* 333(6044):883–885.
28. Blasius TL, Cai D, Jih GT, Toret CP, Verhey KJ (2007) Two binding partners cooperate to activate the molecular motor Kinesin-1. *J Cell Biol* 176(1):11–17.